Title

Identification of the Selective Sites for Electrochemical Reduction of CO to C2+ Products on Copper Nanoparticles by Combining Reactive Force Fields, Density Functional Theory, and Machine Learning

Journal

ACS Energy Letters, 3(12)

ISSN

2380-8195

Authors

Huang, Yufeng
Chen, Yalu
Cheng, Tao
et al.

Publication Date

2018-12-14

DOI

10.1021/acsenergylett.8b01933

Peer reviewed

Identification of the Selective Sites for Electrochemical Reduction of CO to C_{2+} Products on Copper Nanoparticles by Combining Reactive Force Fields, Density Functional Theory, and Machine Learning

Yufeng Huang,[†] Yalu Chen,[†] Tao Cheng,[†] Lin-Wang Wang,[‡] and William A. Goddard, III*,[†]

[†]Materials Simulation Center and Joint Center for Artificial Photosynthesis, California Institute of Technology, Pasadena, California 91125, United States

[‡]Materials Sciences Division, Lawrence Berkeley National Laboratory, Berkeley, California 94720, United States

ABSTRACT: Recent experiments have shown that CO reduction on oxide derived Cu nanoparticles (NP) are highly selective toward C_{2+} products. However, understanding of the active sites on such NPs is limited, because the NPs have ∼200 000 atoms with more than 10 000 surface sites, far too many for direct quantum mechanical calculations and experimental identifications. We show here how to overcome the computational limitation by combining multiple levels of theoretical computations with machine learning. This approach allows us to map the machine learned CO adsorption energies on the surface of the copper nanoparticle to construct the active site visualization (ASV). Furthermore, we identify the structural criteria for optimizing selective reduction by predicting the reaction energies of the potential determining step, ΔE_{OCCOH}, for the C_{2+} product. Based on this structural criterion, we design a new periodic copper structure for CO reduction with a theoretical faradaic efficiency of 97%.

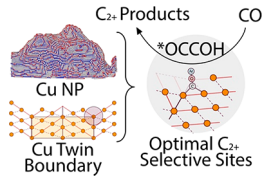

Rapid progress is being made in developing new catalysts that are highly active and selective to electrochemically reduce CO or CO_2 to specific chemical fuels and feedstocks.[1,2] Improved selectivity and activity in reducing CO_2 and CO to valuable hydrocarbons and alcohols will enable the conversion of intermittent or remote renewable energies into complex chemical forms for storage and delivery.[3] At the same time, using sequestrated CO_2 as the feedstock would reduce the amount of excess atmospheric CO_2 by completing the carbon cycle with carbon fixation via artificial photosynthesis or other forms of renewable energy sources.[4,5]

However, CO_2 is quite stable, making it very challenging to optimize catalytic efficiency due to the difficulty in activating CO_2.[6] After decades of development, copper remains the only catalyst that can reduce CO or CO_2 by more than two electrons to generate valuable products in nontrivial amounts. Recently, oxide derived copper nanoparticles (NP) have been shown to greatly improve both the activity and selectivity of CO and CO_2 reduction toward C_{2+} products.[7] Based on early temperature-programmed desorption (TPD) experiments, the improved performance of the oxide derived metal NP was hypothesized to arise from strong CO adsorption sites.[8] However, later experiments have found that selectivity correlated linearly with the grain boundary (GB) density.[9,10] In this work, we focus on elucidating which local Cu structures lead to the optimum properties for CO reduction to C_{2+} products.

We previously used density functional theory (DFT) with full solvent and Grand Canonical techniques to determine the reaction mechanisms for CO reduction to C1 and C2 products on Cu (100) and Cu (111) surfaces, leading to an excellent agreement with experiments (overpotentials within 0.05 V).[11,12] However, the experimental 10 nm NP involves ∼200 000 atoms with ∼10 000 possible surface sites, well beyond the capabilities of DFT. To circumvent the limitation of the direct application of DFT, we subsequently utilized the reactive force field (ReaxFF)[13,14] to computationally grow the 10 nm nanoparticles and then used DFT to sample only 84 surface sites for ΔE_{CO} and 4 surface sites for ΔE_{OCCOH}.[15,16] In order to extract a quantitative understanding of the variations of the chemistry over the whole nanoparticle, we propose here a methodology to combine limited numbers of DFT

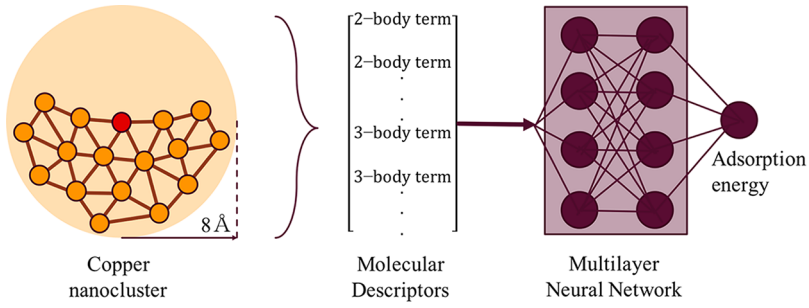

Figure 1. Schematics of the machine learning model. For each surface site (red), we extract a copper cluster including all the atoms within 8 Å from a copper NP. The adsorption energy is calculated using DFT and is used as the target property for training. We use a Behler-Parrinello[17] type neural network model. In this study, we describe the copper cluster by a set of 2-body and 3-body molecular descriptors about the surface atom. We then used these descriptors as input to a multilayer neural network for fitting.

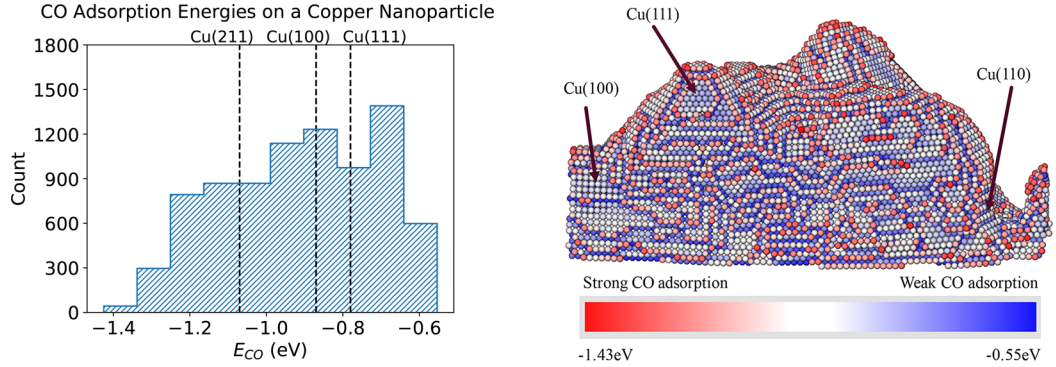

Figure 2. (a) Distribution of CO binding energies (ΔE_{CO}) on the 10 nm copper nanoparticle. The three vertical dashed lines correspond to the CO adsorption energies of single crystal surfaces of (211), (100), and (111).[15] (b) Active site visualization (ASV) of the predicted CO adsorption energies on the nanoparticle. As indicated by the colored bar, the red sites correspond to strong CO adsorption, the white sites correspond to moderate CO adsorption, and the blue sites correspond to weak CO adsorption. The common surfaces of (100), (111), and (110) are indicated in the figure.

calculations with machine learning to train a machine learning model that accurately predicts the binding energies for all sites.

First, we used ReaxFF to computationally synthesize a 10 nm copper nanoparticle (NP) that closely resembles the experimental NP [S1.1 in SI]. The predicted structure leads to XRD spectra and TEM images that match those of the experimental NP structures. Next, we selected 400 random surface sites and calculated their CO adsorption energies using DFT [S1.2 in SI]. We previously found that including atoms up to 8 Å from the surface site is sufficient to represent the local environment.[15] We integrated this local environment into a neural network in which the surrounding atoms are transformed into 12 two-body and 18 three-body molecular descriptors as inputs to a 2-layer neural network with 50 nodes in each layer, as shown in Figure 1. Further details of the descriptor definition are in section S1.3 of the Supporting Information. We partitioned the 400 surface sites into training set, validation set, and test set with an 8:1:1 ratio. Here the validation set is used to terminate the training sufficiently early to avoid overfitting. Section S2 of the Supporting Information shows that the root mean squared error (RMSE) of the CO binding energy (ΔE_{CO}) on the training set is 0.111 eV while for the validation set RMSE = 0.117 eV and for the test set RMSE = 0.123 eV. We refer to this as the ReaxQM-Machine Learning strategy, or RxQM-ML. This is much lower than the RMSE = 0.2 eV for a similar study of the crystalline surface of the NiGa binary alloy.[18]

After training this accurate neural network model, we use RxQM-ML to predict the CO adsorption energies for all 10 000 surface sites. The statistical distribution of the CO adsorption energies is shown in Figure 2a. Overall, the CO adsorptions range from −0.55 to −1.43 eV, showing the wide variety of surface sites on the copper NP. As expected, most energies are clustered around the values for such low index surfaces, as (111), (100), and (211).[15] However, we find a significant number of surface sites with much stronger CO adsorption energies. This is shown by the distribution to the left of the (211) line. These results are consistent with the TPD experiments, which show a broad peak centered at 275 K only for the copper NP, indicating that ∼7−15% of the surface leads to stronger CO adsorptions than low index copper surfaces.[8]

Furthermore, the low cost of the RxQM-ML model makes it possible to establish the quantitative structure−activity relationship (QSAR) such that the machine-learned CO adsorption energies can be remapped back to the copper nanoparticle, as shown in Figure 2b. Here red indicates low ΔE_{CO}, white indicates moderate ΔE_{CO}, and blue indicates unfavorable ΔE_{CO}. The (100), (111), and (110) surfaces are all colored light blue, indicating that they are near the mean values of the adsorption energy distributions as in Figure 2a.

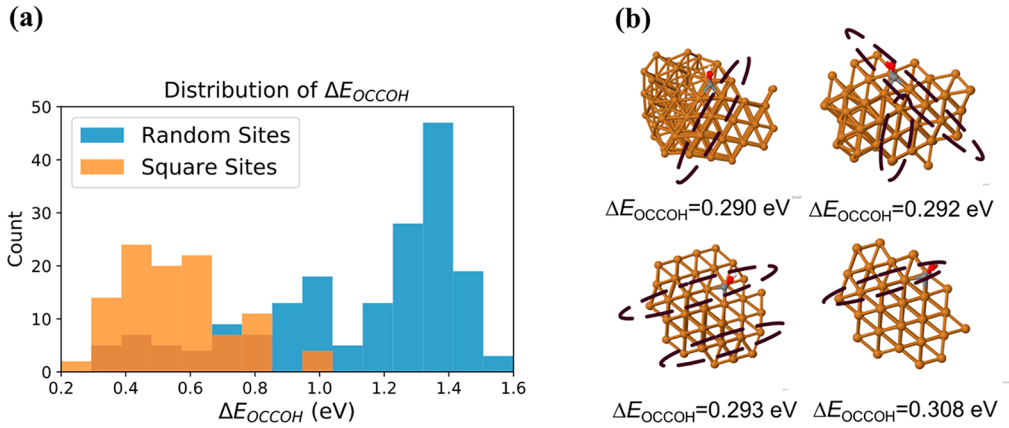

Figure 3. (a) Distributions of ΔE_{OCCOH} on the surface of the copper nanoparticle. Blue: 180 *random* surface sites; orange: 100 random *square* sites. (b) The four square structures with the lowest ΔE_{OCCOH} sampled randomly from the copper nanoparticle. The dashed ellipses indicate the locations of the twin boundaries.

The sites in solid blue are not fully exposed, making them difficult for CO to bind. The sites in red are of the greatest interest because they correspond to more favorable adsorptions of CO than the low-index surfaces. As shown in light red in the figure, the moderately strong CO adsorption sites are typically along the step edges, and as shown in solid red, the strong CO adsorption sites are mostly isolated surface sites or kink sites.

The ASV in Figure 2 shows clearly that favorable CO adsorption sites are scattered across the whole nanoparticle surface. This is consistent with experimental observations that the surface areas corresponding to GBs are not sufficiently large to account for the number of strong CO adsorption sites.[8] Using RxQM-ML, we now directly show that the strong CO adsorption energies are not just at GBs.

Although we have demonstrated that the CO binding energy is not necessary to correlate with GBs, there is a great deal of experimental evidence suggesting that increasing the GB density can significantly improve the C_{2+} selectivity. Another descriptor is needed to describe selectivity of these nanoparticles. As shown experimentally[19] and theoretically,[20−22] the selective step toward C_{2+} products involves C−C coupling in which *OCCOH is formed. Thus, the most plausible descriptor is the reaction energy for forming *OCCOH

$$\Delta E_{OCCOH} = E[*OCCOH] - E[*CO,*CO] - 0.5 \times E[H_2]$$

which we have shown previously to be the potential determining step for ethanol production.

Then, we started with ∼180 randomly sampled surface sites and calculated the formation energy for *OCCOH, ΔE_{OCCOH}. The distribution is shown in the blue histograms in Figure 3a. As shown in the figure, the range of ΔE_{OCCOH} spans by more than 1 eV, implying that some sites are much more selective than others. We could sample additional sites to develop a similar machine learning model for ΔE_{OCCOH}. However, we examine the sites with the lowest ΔE_{OCCOH}, and found that all of them involve square sites, similar to those of the (100) surface. To test this hypothesis, we further sampled 100 ***square*** sites, leading to the distribution for ΔE_{OCCOH} shown in orange in Figure 3a. Comparing to the random sites on the surface of the copper nanoparticle, we find that the square sites are indeed more favorable, as shown by the shift in the distribution in ΔE_{OCCOH} in Figure 3a.

With the new distribution of just the ***square*** sites, we extracted the common features of the most selective sites by further examining the square sites with the lowest ΔE_{OCCOH}. We found that a step (111) surface is always next to these favorable square sites, as shown in the Figure 3b. These sites are similar to the Cu(S)[n(100) × (111)] edge step sites where the (111) surface and the (100) surface intersect. In fact, experiments[23,24] showed that these step sites have higher selectivity than either the (100) and (111) surface. To confirm this theoretically, we calculated ΔE_{OCCOH} on (100), (111), (311), and (511) surfaces to be 0.44, 0.64, 0.52, and 0.41 eV. The calculated trend agrees very well with the experimental selectivity trend in which (511) > (100) > (311) > (111) (Section S3 in SI). This comparison with experimental findings on the Cu(S)[n(100) × (111)] surfaces confirms the validity of using E_{OCCOH} as the descriptor for the selectivity toward C_{2+} products. It is also consistent with our finding from sampling the NP that favorable sites for ΔE_{OCCOH} or C_{2+} selectivity must involve a (111) step surface next to a (100) site where *OCCOH is formed.

In addition, twin boundaries are associated with the square surface sites having the lowest ΔE_{OCCOH}. Figure 3b shows that these twin boundaries are all next to the site where *OCCOH is formed. This implies that the selectivity toward C_{2+} products are directly related to twin boundaries which are a special type of GBs.

Building on the idea that the above common features lead to the best *OCCOH sites, we constructed the smallest periodic structure possessing these features. This is shown in Figure 4. We expect that this periodic surface will behave chemically in the same way as these selective sites. Because it is a smallest periodic structure containing these sites, the density of active sites will be much higher than the randomly and sparsely distributed active sites on a nanoparticle.

This minimal periodic structure is shown in Figure 4a. From the ABC stacking of the FCC copper, the smallest grain size must be at least 6 layers wide, corresponding to ABCACB stacking, where the A layers are twin boundaries. Since the step surfaces involving the (100) and (111) are of interest, they are shown by double lines and dashed lines in the figure.

Based on the configurations of the adsorbed *OCCOH on the copper clusters, there are 4 ways of placing the

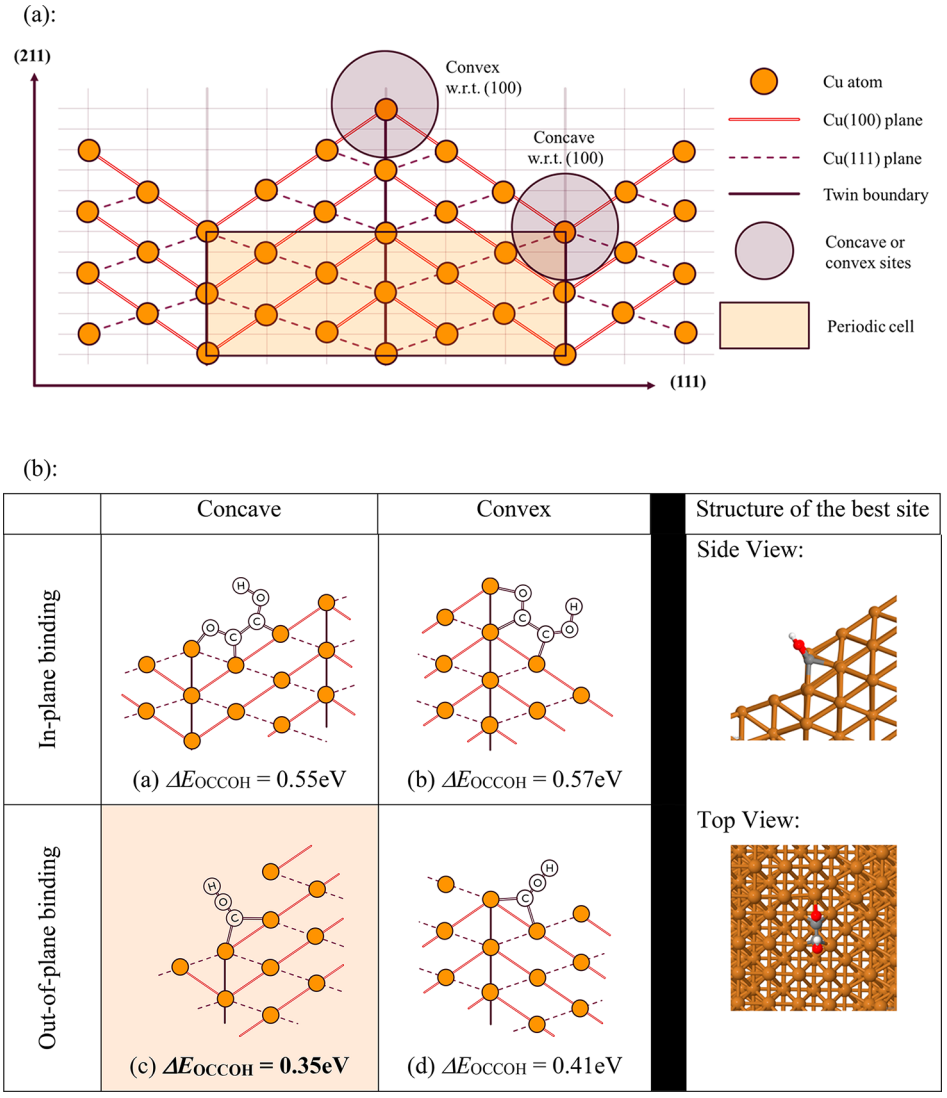

Figure 4. (a) The shaded area is the minimal periodic structure of FCC copper containing the (100) planes, (111) planes, and twin boundaries. Terminating this structure to expose the (100) and (111) surfaces leads to sites that are concave or convex with respect to the (100) planes. (b) The four types of sites for adsorbed *OCCOH on the surface of the minimal periodic structure. The structure that is concave with respect to the (100) planes has the most favorable ΔE_{OCCOH} for C_{2+} selectivity. The top and side views of this structure are shown on the right column of (b). More details on these sites are shown in section S4 of the Supporting Information. Note that for structures (c) and (d), the other carbon and oxygen atoms are not shown since they overlap with the foreground atoms in the side view. The full *OCCOH structure for (c) is revealed in the top view, as shown on the right column.

intermediate on this surface, as shown in Figure 4b. The first two structures, (a) and (b), with the *OCCOH adsorbed in the cross-sectional plane show unfavorable energies. Thus, the in-plane *OCCOH adsorption is not responsible for the increased in C_{2+} selectivity. On the other hand, *OCCOH adsorbed perpendicular to the page (or out-of-plane) are much more favorable, with only 0.41 eV for the convex site and 0.35 eV for the concave site, which is better than all the single crystal surface sites considered here. In fact, the same configuration is also found for the copper nanoparticle. As shown again in Figure 3b, *OCCOH are all adsorbed perpendicular to the page. Thus, we predict that the (100)-like square sites next to a (111)-like step surface and on-top of a twin boundary that binds *OCCOH parallel to the twin boundary will have the most favorable ΔE_{OCCOH}, which corresponds to the most selective sites.

For the most favorable structure, the faradaic efficiency toward C_{2+} product is predicted to be 97% using experimental data in which the current density for C_{2+} production increases linearly as the density of GBs, and the current for hydrogen production remains the same.[10] The prediction is shown in Figure 5, which also includes a prediction for an experimental copper structure in which a high density of twin boundaries is synthesized,[25] assuming that the structure is exposing the twin boundaries in the preferable configuration. Details of this prediction is summarized in section S4 of the Supporting Information.

In conclusion, we used machine learning to fit the structure–activity relationship between the local structures of the copper nanoparticle and the theoretical CO adsorption energies. By extrapolating the energies back to the nanoparticle, we found that strong CO adsorption energies are not just on GBs, implying that CO adsorption energies are not an

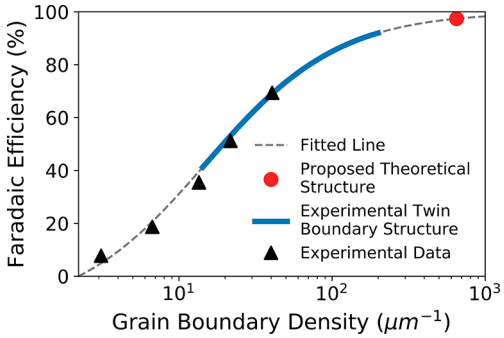

Figure 5. Predicted faradaic efficiency (FE) of the concave site on the minimal periodic structure compared to experimental data. An experimental copper structure with abundant twin boundaries[25] are also extrapolated based on the densities of the boundaries.

appropriate descriptor for C_{2+} selectivity. Rather, we show that ΔE_{OCCOH}, the transition state for forming ethanol of C_{2+} products in C−C coupling, is the appropriate descriptor. This explains the selectivity on Cu(S)[n(100) × (111)] surfaces and the twin-related step square sites on the nanoparticle. To illustrate how to use this information, we designed the minimal periodic structure. This minimal periodic structure has a super high density of selective sites that we expect will lead to near unity selectivity based on extrapolations of theoretical and experimental data.

AUTHOR INFORMATION

Corresponding Author

*E-mail: wag@caltech.edu.

ORCID

Yufeng Huang: 0000-0002-0373-2210

Tao Cheng: 0000-0003-4830-177X

William A. Goddard, III: 0000-0003-0097-5716

Notes

The authors declare no competing financial interest.

ACKNOWLEDGMENTS

This work was supported by the Joint Center for Artificial Photosynthesis, a DOE Energy Innovation Hub, supported through the Office of Science of the U.S. Department of Energy under Award Number DE-SC0004993. This material is also based upon work supported by the U.S. Department of Energy, Office of Science, Office of Workforce Development for Teachers and Scientists, Office of Science Graduate Student Research (SCGSR) program. The SCGSR program is administered by the Oak Ridge Institute for Science and Education for the DOE under contract number DE-SC0014664. This work uses the resource of National Energy Research Scientific Computing center (NERSC).

REFERENCES

(1) Zhang, W.; Hu, Y.; Ma, L.; Zhu, G.; Wang, Y.; Xue, X.; Chen, R.; Yang, S.; Jin, Z. Progress and Perspective of Electrocatalytic CO_2 Reduction for Renewable Carbonaceous Fuels and Chemicals. *Adv. Sci.* **2018**, *5* (1), 1700275.

(2) Zhao, G.; Huang, X.; Wang, X.; Wang, X. Progress in Catalyst Exploration for Heterogeneous CO_2 Reduction and Utilization: A Critical Review. *J. Mater. Chem. A* **2017**, *5* (41), 21625−21649.

(3) Detz, R. J.; Reek, J. N. H.; Van Der Zwaan, B. C. C. The Future of Solar Fuels: When Could They Become Competitive? *Energy Environ. Sci.* **2018**, *11* (7), 1653−1669.

(4) Van Der Giesen, C.; Kleijn, R.; Kramer, G. J. Energy and Climate Impacts of Producing Synthetic Hydrocarbon Fuels from CO_2. *Environ. Sci. Technol.* **2014**, *48* (12), 7111−7121.

(5) Artz, J.; Müller, T. E.; Thenert, K.; Kleinekorte, J.; Meys, R.; Sternberg, A.; Bardow, A.; Leitner, W. Sustainable Conversion of Carbon Dioxide: An Integrated Review of Catalysis and Life Cycle Assessment. *Chem. Rev.* **2018**, *118* (2), 434−504.

(6) Kumar, B.; Llorente, M.; Froehlich, J.; Dang, T.; Sathrum, A.; Kubiak, C. P. Photochemical and Photoelectrochemical Reduction of CO_2. *Annu. Rev. Phys. Chem.* **2012**, *63*, 541−569.

(7) Li, C. W.; Kanan, M. W. CO_2 Reduction at low Overpotential on Cu Electrodes Resulting from the Reduction of Thick Cu_2O Films. *J. Am. Chem. Soc.* **2012**, *134* (17), 7231−7234.

(8) Verdaguer-Casadevall, A.; Li, C. W.; Johansson, T. P.; Scott, S. B.; McKeown, J. T.; Kumar, M.; Stephens, I. E. L.; Kanan, M. W.; Chorkendorff, I. Probing the Active Surface Sites for CO Reduction on Oxide-Derived Copper Electrocatalysts. *J. Am. Chem. Soc.* **2015**, *137* (31), 9808−9811.

(9) Feng, X.; Jiang, K.; Fan, S.; Kanan, M. W. Grain-Boundary-Dependent CO_2 Electroreduction Activity. *J. Am. Chem. Soc.* **2015**, *137* (14), 4606−4609.

(10) Feng, X.; Jiang, K.; Fan, S.; Kanan, M. W. A Direct Grain-Boundary-Activity Correlation for CO Electroreduction on Cu Nanoparticles. *ACS Cent. Sci.* **2016**, *2* (3), 169−174.

(11) Nørskov, J. K.; Bligaard, T.; Rossmeisl, J.; Christensen, C. H. (2009). Towards the Computational Design of Solid Catalysts. *Nat. Chem.* **2009**, *1* (1), 37−46.

(12) Becke, A. D. Perspective: Fifty Years of Density-Functional Theory in Chemical Physics. *J. Chem. Phys.* **2014**, *140* (18), 18A301.

(13) van Duin, A. C. T.; Dasgupta, S.; Lorant, F.; Goddard, W. A. ReaxFF: A Reactive Force Field for Hydrocarbons. *J. Phys. Chem. A* **2001**, *105* (41), 9396.

(14) Chenoweth, K.; van Duin, A. C. T.; Goddard, W. A. ReaxFF Reactive Force Field for Molecular Dynamics Simulations of Hydrocarbon Oxidation. *J. Phys. Chem. A* **2008**, *112* (5), 1040−1053.

(15) Cheng, T.; Xiao, H.; Goddard, W. A. Nature of the Active Sites for CO Reduction on Copper Nanoparticles; Suggestions for Optimizing Performance. *J. Am. Chem. Soc.* **2017**, *139* (34), 11642−11645.

(16) Cheng, T.; Huang, Y.; Xiao, H.; Goddard, W. A. Predicted Structures of the Active Sites Responsible for the Improved Reduction of Carbon Dioxide by Gold Nanoparticles. *J. Phys. Chem. Lett.* **2017**, *8* (14), 3317−3320.

(17) Behler, J.; Parrinello, M. Generalized Neural-Network Representation of High-Dimensional Potential-Energy Surfaces. *Phys. Rev. Lett.* **2007**, *98* (14), 1−4.

(18) Ulissi, Z. W.; Tang, M. T.; Xiao, J.; Liu, X.; Torelli, D. A.; Karamad, M.; Cummins, K.; Hahn, C.; Lewis, N. S.; Jaramillo, T. F.; Chan, K.; Nørskov, J. K. Machine-Learning Methods Enable Exhaustive Searches for Active Bimetallic Facets and Reveal Active Site Motifs for CO_2 Reduction. *ACS Catal.* **2017**, *7* (10), 6600−6608.

(19) Pérez-Gallent, E.; Figueiredo, M. C.; Calle-Vallejo, F.; Koper, M. T. M. Spectroscopic Observation of a Hydrogenated CO Dimer Intermediate During CO Reduction on Cu(100) Electrodes. *Angew. Chem., Int. Ed.* **2017**, *56* (13), 3621−3624.

(20) Calle-Vallejo, F.; Koper, M. T. M. Theoretical Considerations on the Electroreduction of CO to C_2 Species on Cu(100) Electrodes. *Angew. Chem.* **2013**, *125* (28), 7423−7426.
(21) Cheng, T.; Xiao, H.; Goddard, W. A. Full Atomistic Reaction Mechanism with Kinetics for CO Reduction on Cu(100) from ab initio Molecular Dynamics Free-Energy Calculations at 298 K. *Proc. Natl. Acad. Sci. U. S. A.* **2017**, *114* (8), 1795−1800.
(22) Xiao, H.; Cheng, T.; Goddard, W. A. Atomistic Mechanisms Underlying Selectivities in C_1 and C_2 Products from Electrochemical Reduction of CO on Cu(111). *J. Am. Chem. Soc.* **2017**, *139* (1), 130−136.
(23) Hori, Y.; Takahashi, I.; Koga, O.; Hoshi, N. Selective Formation of C2 Compounds from Electrochemical Reduction of CO_2 at A Series of Copper Single Crystal Electrodes. *J. Phys. Chem. B* **2002**, *106* (1), 15−17.
(24) Kim, Y. G.; Javier, A.; Baricuatro, J. H.; Torelli, D.; Cummins, K. D.; Tsang, C. F.; Hemminger, J. C.; Soriaga, M. P. Surface Reconstruction of Pure-Cu Single-Crystal Electrodes under CO-Reduction Potentials in Alkaline Solutions: A Study by Seriatim ECSTM-DEMS. *J. Electroanal. Chem.* **2017**, *793*, 113−118.
(25) Morris Wang, Y.; Sansoz, F.; Lagrange, T.; Ott, R. T.; Marian, J.; Barbee, T. W.; Hamza, A. V. Defective Twin Boundaries in Nanotwinned Metals. *Nat. Mater.* **2013**, *12* (8), 697−702.